Online chatter monitoring and suppression in robotic machining systems

Zhen Zhu[a], Pingfa Feng[a,b], Heng Wu[a], Jie Xu[a], Julian Blumberg[c], Enlai Jiang [a], Eckart Uhlmann[c], Feng Feng[a,*]

[a] *Lab for Intelligent Manufacturing Equipment and Systems, Shenzhen International Graduate School, Tsinghua University, Shenzhen 518055, China*

[b] *Department of Mechanical Engineering, Tsinghua University, Beijing 100084, China*

[c] *Institute for Machine Tools and Factory Management, Technische Universität Berlin, Berlin D-10587, Germany*

Correspondence (F. Feng): E-mail: feng.feng@sz.tsinghua.edu.cn; ORCID: 0000-0002-3960-7761.

Abstract

Industrial robots are increasingly used in milling tasks across aerospace, mold manufacturing, and other industries due to their high flexibility, ease of integration, and large workspace. However, their inherent low stiffness makes them susceptible to chatter vibrations, which significantly impact machining stability and part quality. This study presents a novel online chatter monitoring and suppression system that integrates real-time chatter detection with adaptive spindle speed variation (SSV). High-frequency triaxial accelerometers are employed to capture tool vibration data, which is processed using Fast Fourier Transform (FFT) and a frequency-domain notch filter to identify and eliminate spindle rotation frequency, tooth passing frequency, and their harmonics, enabling precise chatter frequency detection. Based on real-time chatter frequency identification, an adaptive spindle speed variation strategy is proposed to suppress vibration by adjusting the spindle speed to a stable zone. Experimental results show that the system responds within 100 ms once the vibration threshold is exceeded, with the total monitoring-to-suppression process taking approximately 1.6 s, and the suppression strategy reducing vibration amplitude by over 80%. This significantly enhances the stability and robustness of robotic milling. Additionally, experimental comparisons with conventional CNC machines demonstrate that by optimizing robot end-effector stiffness and process parameters, robotic milling stability improves, achieving surface roughness of approximately Ra 2 µm. The system's chatter suppression success rate exceeds 90%, improving surface quality by about 60% and increasing machining efficiency by over 30%. The developed system’s real-time performance and adaptive capabilities suggest its potential for integration into advanced manufacturing systems, offering a promising framework for incorporating online chatter monitoring and suppression into smart manufacturing environments.

Keywords: Milling chatter; Industrial robot; Spindle speed variation; Online chatter monitoring and suppression.

1 Introduction

Chatter is a major barrier to productivity and quality in milling, especially for thin-walled components in aerospace and other high-value manufacturing. Its regenerative mechanism has been well studied, and stability lobe diagrams (SLDs) are widely used to select nominally stable cutting conditions. However, SLDs are based on fixed dynamics, while in practice chatter frequencies shift with tool wear, thermal drift, and process variations. As a result, offline predictions alone often fail to prevent instability. This highlights the need for an online monitoring and suppression strategy that can detect chatter onset in real time and respond quickly enough to restore stability.

Efforts toward online chatter monitoring illustrate both progress and limitations. Early analytical approaches, such as the stability lobe diagram (SLD) method proposed by Merritt [1], provided a theoretical foundation for chatter prediction by relating spindle speed and depth of cut to stability regions. This was later refined by Das and Tobias [2], who incorporated dynamic force variations with chip thickness, and by Tlusty [3], who emphasized the force–displacement interaction mechanism. Chandiramani and Pothala [4] further developed two-degree-of-freedom models for turning, showing how increased width of cut may destabilize the process. Finite element methods were also explored, for instance by Wang and Cleghorn [5], who analyzed rotating shaft stability using Nyquist criteria, and Mahdavinejad [6], who incorporated tool–workpiece–machine flexibility into predictive models. While these analytical and numerical studies advanced theoretical understanding, their reliance on accurate structural models limits industrial feasibility.

Signal-based chatter detection remains more practical, exploiting cutting force, vibration, or acoustic emission data. Tangjitsitcharoen [7,8] introduced power spectral density (PSD) analysis to discriminate between continuous cutting, tool breakage, and chatter states. Shi et al. [9] demonstrated that acceleration signals perpendicular to feed are more sensitive to chatter than parallel ones, while Gradišek et al. [10] compared force and sound signals in grinding and confirmed the diagnostic potential of acoustic sensing, albeit with delays. Classical frequency-domain analysis via FFT [11] remains efficient, but chatter peaks are often masked by tooth-passing harmonics. Wavelet-based and Hilbert–Huang methods [11,12] provide superior time–frequency localization, though their computational overhead impedes real-time deployment. More recently, artificial intelligence methods have gained momentum. Tarng et al. [13] first applied neural networks to thrust spectrum analysis in drilling, while Arriaza [14] extended ANN to multisensor fusion for chatter detection. SVM classifiers combined with wavelet features have also shown high accuracy, as in Yao et al. [15]. Vision-based detection has been demonstrated by Lei and Soshi [16] and Khalifa et al. [17]. Deep learning has further enhanced capability: Zhu et al. [18] employed CNNs with genetic algorithms for image-based chatter recognition, and Rahimi et al. [19] hybridized CNNs with physical models to improve classification robustness. However, machine learning methods still demand large labeled datasets and generalize poorly across machining conditions, and their black-box nature reduces interpretability.

Once chatter is identified, the subsequent challenge is suppression. Approaches here can be broadly divided into passive, active, and spindle speed variation (SSV) methods. Passive suppression enhances damping or stiffness. Marui et al. [20], Kim et al. [21], and Madoliat et al. [22,23] designed friction-based damping toolholders, while Galarza et al. [24] and Saciotto et al. [25] employed impact absorbers. Tuned mass dampers (TMDs) developed by Saadabad et al. [26] and Ma et al. [27,28] have demonstrated effectiveness but suffer from tuning complexity and space constraints. Active control relies on actuators to counteract vibrations in real time. Zhang et al. [29] implemented piezo-actuated toolholders, Monnin et al. [30] designed active spindles with piezo/electromagnetic actuation, and Möhring [31] developed active workpiece fixtures. Wan et al. [32,33] and Du et al. [34] further advanced electromagnetic actuator systems for chatter suppression. These achieve precise suppression but require costly hardware and complex integration.

In contrast, SSV disrupts the regenerative effect by modulating spindle speed. Continuous SSV, as analyzed by Zhang and Ni [35], Zatarain et al. [36], and Albertelli et al. [37], can enlarge stability lobes, with further refinements such as multi-harmonic SSV proposed by Wang et al. [38]. Nam et al. [39] and Li et al. [40] clarified chatter growth characteristics and transition phases in speed variation. Discrete SSV, pioneered by Smith and Tlusty [41] and improved by Liao and Young [42] using FFT-based frequency tracking, offers simpler implementation by stepwise shifting spindle speed upon chatter detection. Adaptive schemes, such as Han [43] using fuzzy control for thin-wall milling and Yamato et al. [44] with sensorless monitoring, further enhance flexibility. Nonetheless, both continuous and discrete SSV depend critically on accurate and timely chatter frequency identification, with detection delays directly impairing effectiveness.

Despite these advances, integration of chatter monitoring and suppression into unified online control systems remains limited. Monitoring alone provides diagnostics without remedy, while suppression alone lacks precision without detection. Recent integrated systems have attempted to bridge this gap. For example, Xiong et al. [45] realized wavelet-entropy-based turning chatter detection with adaptive spindle modulation but relied on costly hardware and lacked quantified suppression. Sun [46] developed a Siemens 840D closed-loop platform with detection leads of 0.2–1 s yet without reporting suppression duration. In milling, Van Dijk et al. [47] tracked chatter onset before visible marks but suffered from spindle loop delays and did not provide full-chain suppression metrics, while Morita [48] achieved suppression through spindle speed adjustment within about 1 s, essentially reflecting spindle acceleration and deceleration limits rather than an explicitly quantified detection–suppression chain. Although promising, such integrated systems still face critical shortcomings. They often depend on closed or costly CNC hardware, their response is constrained by spindle acceleration and controller delays, and suppression effectiveness is rarely quantified. These limitations highlight the need for integrated monitoring–suppression solutions that are fast, lightweight, interpretable, and deployable across diverse machining platforms.

To address these challenges, this study develops an integrated FFT–SSV framework for chatter monitoring and suppression on an ABB IRB6700 robotic milling system. Unlike conventional CNC platforms with closed architectures, the robotic system offers an open spindle control interface that simplifies real-time intervention and facilitates direct deployment of monitoring and control algorithms. Within this framework, a frequency-domain FFT–notch method isolates chatter frequencies in real time for rapid onset detection, while an adaptive spindle speed variation strategy dynamically adjusts spindle speed to restore stability. By combining FFT-based monitoring with SSV suppression in a closed loop, the framework achieves both responsiveness and adaptability, as illustrated in Fig. 1. The framework is first validated through numerical simulations of a delay-differential milling model, and then experimentally tested, with performance evaluated in terms of detection latency, suppression effectiveness, vibration reduction, and surface quality improvement. Results demonstrate that the framework achieves chatter detection in 0.3 s and full suppression in 1.6 s with 100% success rate and over 90% vibration reduction, providing a lightweight, reliable, and directly deployable solution for real-time industrial chatter control.

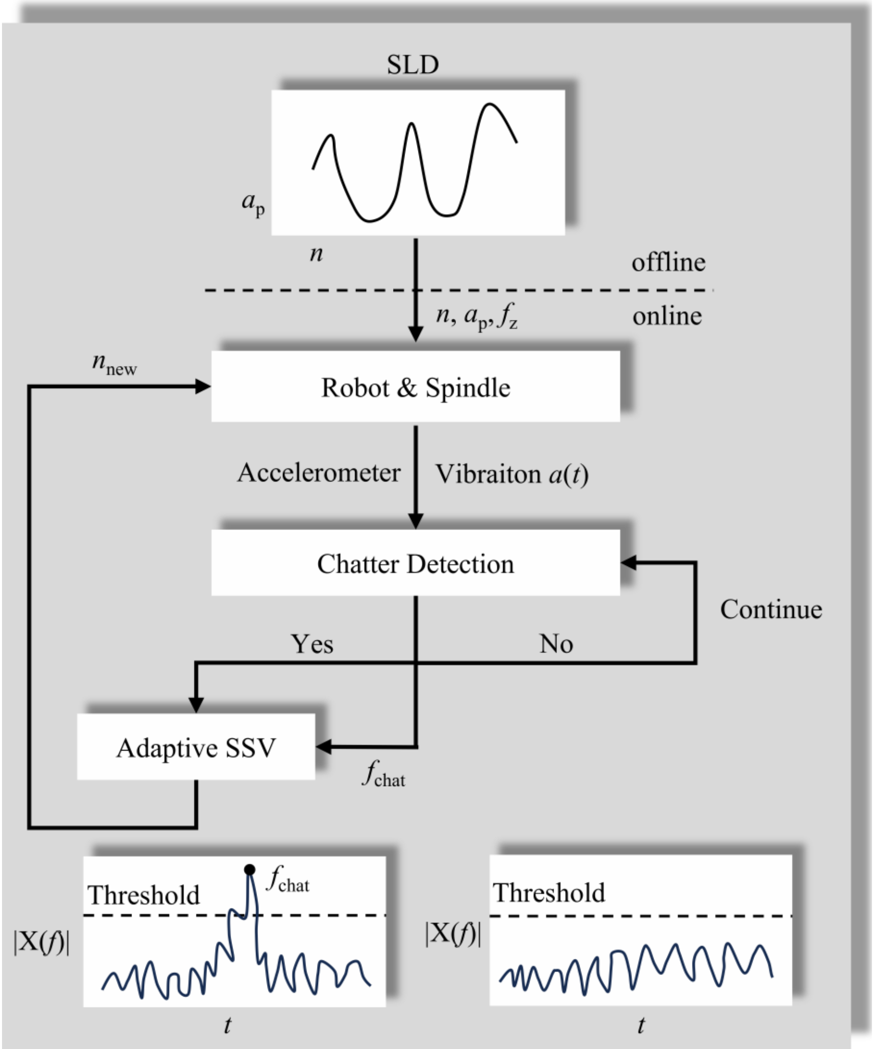

Fig. 1. Framework of chatter detection and suppression in milling using adaptive SSV

The remainder of this paper is organized as follows. Section 2 details the proposed methods, including theoretical modeling of milling dynamics, real-time chatter monitoring, and adaptive spindle speed variation, as well as the experimental setup. Section 3 presents numerical and experimental results, demonstrating chatter identification and suppression performance. Section 4 summarizes the conclusions and discusses the broader implications of the framework.

2 Methods

Chatter in milling originates from the regenerative effect: each tooth cuts a surface already modified by the vibration of previous teeth, introducing a time delay into the dynamics. Explicit modeling of this regenerative mechanism is essential to explain why chatter emerges, how its frequency content can be identified in real time, and why adjusting spindle speed through spindle speed variation (SSV) can suppress instability.

Milling dynamics can be described by four coupled models: chip thickness, cutting forces, spindle–holder–tool structural dynamics, and the resulting time-delay differential equation (DDE) that captures the regenerative effect. Chatter frequency characteristics further link these models to spectral features such as spindle harmonics, tooth-passing harmonics, and off-harmonic peaks, which enable real-time monitoring and suppression.

2.1 Theoretical modeling of milling dynamics

2.1.1 Chip thickness model

Milling is inherently a periodic cutting process. Once the tooth trajectory is defined, the j_{th} tooth has a well-defined static chip thickness $h_{j,\,\mathrm{stat}}(t)$, which depends on the feed per tooth f_{z} and its instantaneous angular position $\phi_j(t)$, and can be formalized as

$$h_{j,\mathrm{stat}}(t) = f_{\mathrm{z}} \sin \phi_j(t) \tag{1}$$

In practice, elastic deformation causes the tool to deviate from its nominal path, introducing a dynamic chip thickness $h_{j,\mathrm{dyn}}(t)$. It is defined as the difference between the instantaneous tool-tip displacement $\boldsymbol{v}(t)=[v_x(t),v_y(t)]^{\mathrm{T}}$ and the displacement one tooth period earlier $\boldsymbol{v}(t\text{-}\tau)$, with the regenerative delay $\tau = 60/(zn)$ set by spindle speed n and tooth number z:

$$h_{j,\mathrm{dyn}}(t) = [\sin \phi_j(t) \quad \cos \phi_j(t)]\big(\boldsymbol{v}(t) - \boldsymbol{v}(t-\tau)\big) \tag{2}$$

The total instantaneous chip thickness is then

$$h_j(t) = h_{j,\mathrm{stat}}(t) + h_{j,\mathrm{dyn}}(t) \tag{3}$$

This formulation underscores the regenerative effect: the vibration displacement of a current tooth is compared with that of a previous tooth delayed by τ. The resulting wavy surface on the workpiece left by the preceding tooth, which governs the instantaneous chip thickness of the following tooth, is shown in Fig. 2. In this schematic, v_0 denotes the surface waviness generated by the previous cutting pass, v represents the vibration trajectory of the current tooth, and their misalignment $\Delta l(\varepsilon)$ reflects the degree of overlap between successive waves as determined by the phase shift ε. In the time domain, this appears as an explicit delay term, while in the frequency domain, the delay manifests as a phase factor $\mathrm{e}^{i\omega\tau}$.

Hence, τ corresponds to a phase shift $\varepsilon = \omega\tau$. Constructive interference ($\varepsilon = 0$) reinforces chatter, while destructive interference ($\varepsilon = \pi$) suppresses it, as illustrated in Fig. 3. This interpretation establishes the theoretical link between spindle speed and the regenerative stability of milling through the delay term τ. To capture the resulting forces that drive vibrations, this chip thickness model is next coupled with a cutting force formulation.

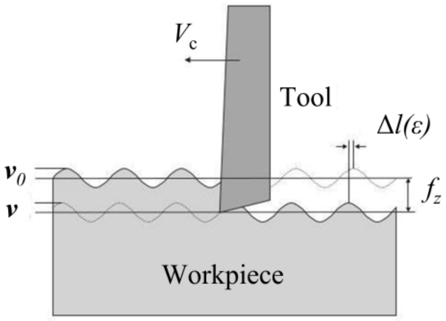

Fig. 2. Wavy surface of workpiece in orthogonal cutting

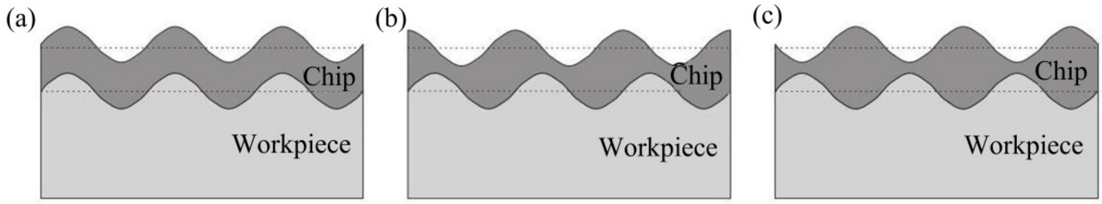

Fig. 3. Effect of phase difference on dynamic chip thickness
(a) $\varepsilon = 0$. (b) $\varepsilon = 1/2\ \pi$. (c) $\varepsilon = \pi$.

2.1.2 Cutting force model

Cutting forces are modeled empirically as nonlinear functions of chip thickness $h_j(t)$. For the j_{th} tooth, tangential and radial forces are expressed as

$$\begin{aligned} F_{\mathrm{tang},j}(t) &= g_j\left(\phi_j(t)\right) K_{\mathrm{t}} a_{\mathrm{p}} h_j(t)^{x_F} \\ F_{\mathrm{rad},j}(t) &= g_j\left(\phi_j(t)\right) K_{\mathrm{r}} a_{\mathrm{p}} h_j(t)^{x_F} \end{aligned} \tag{4}$$

where a_{p} is the axial depth of cut, K_{t} and K_{r} are cutting coefficients, and x_F (typically 0.8–1.0) characterizes the nonlinear dependence on chip thickness. The switching function $g_j(\phi_j(t))$ equals 1 when the tooth is engaged ($\phi_s \leq \phi_j(t) \leq \phi_e$) and zero otherwise.

Using coordinate transformations, these local forces are expressed in the global machine coordinate system. Summing over all z teeth yields the total cutting force vector:

$$\mathbf{F}(t) = a_{\mathrm{p}} \sum_{j=0}^{z-1} g_j\left(\phi_j(t)\right)\left(h_{j,\mathrm{stat}}(t) + h_{j,\mathrm{dyn}}(t)\right)^{x_F} \boldsymbol{S}(t) \begin{bmatrix} K_{\mathrm{t}} \\ K_{\mathrm{r}} \end{bmatrix} \tag{5}$$

where $\boldsymbol{S}(t)$ is a geometric transformation matrix defined by the angular position $\phi_j(t)$. For clarity, the cutter is assumed to have straight flutes with zero helix angle, so only the feed (x) and normal (y) directions are considered.

$$\boldsymbol{S}(t)=\begin{bmatrix}-\cos\phi_j(t) & -\sin\phi_j(t)\\ \sin\phi_j(t) & -\cos\phi_j(t)\end{bmatrix} \tag{6}$$

2.1.3 Spindle–holder–tool dynamics

The spindle–holder–tool system is modeled as a two-degree-of-freedom mass–spring–damper oscillator in the feed (x) and normal (y) directions, as illustrated in Fig. 4. For reference, a schematic of the physical spindle–holder–tool assembly is shown in Fig. 5. In state-space form, the dynamics are expressed as:

$$\begin{aligned}\dot{\boldsymbol{x}}(t)&=\boldsymbol{A}\boldsymbol{x}(t)+\boldsymbol{B}\boldsymbol{u}(t),\\ \boldsymbol{y}(t)&=\mathbf{C}\boldsymbol{x}(t)+\mathbf{D}\boldsymbol{u}(t)\end{aligned} \tag{7}$$

where $\boldsymbol{u}(t)=\boldsymbol{F}(t)$ is the cutting-force input, and the output $\boldsymbol{y}(\mathrm{t})=\boldsymbol{v}(t)=[v_x(t), v_y(t)]^{\mathrm{T}}$ is the tool-tip displacement. Assuming the two directions are uncoupled, the state vector for each direction is $\boldsymbol{x}_i(t)=[v_i(t), \dot{v}_i(t)]^{\mathrm{T}}$ ($i=x,y$), with matrices:

$$\boldsymbol{A}_i=\begin{bmatrix}0 & 1\\ -\dfrac{k_i}{m_i} & -\dfrac{b_i}{m_i}\end{bmatrix},\quad \boldsymbol{B}_i=\begin{bmatrix}0\\ \dfrac{1}{m_i}\end{bmatrix},\quad \mathbf{C}_i=\begin{bmatrix}1 & 0\end{bmatrix},\quad \mathbf{D}_i=\mathbf{0},$$

where m_i, b_i, and k_i denote modal mass, damping, and stiffness, respectively. These parameters can be identified experimentally or by finite element analysis.

This compact representation integrates directly with the chip-thickness and cutting-force models, providing the displacement response $\boldsymbol{v}(t)$ that drives the regenerative term. More complex cases (cross-coupling, speed-dependent stiffness, or workpiece flexibility) can be accommodated by expanding the matrices in Eq. (7).

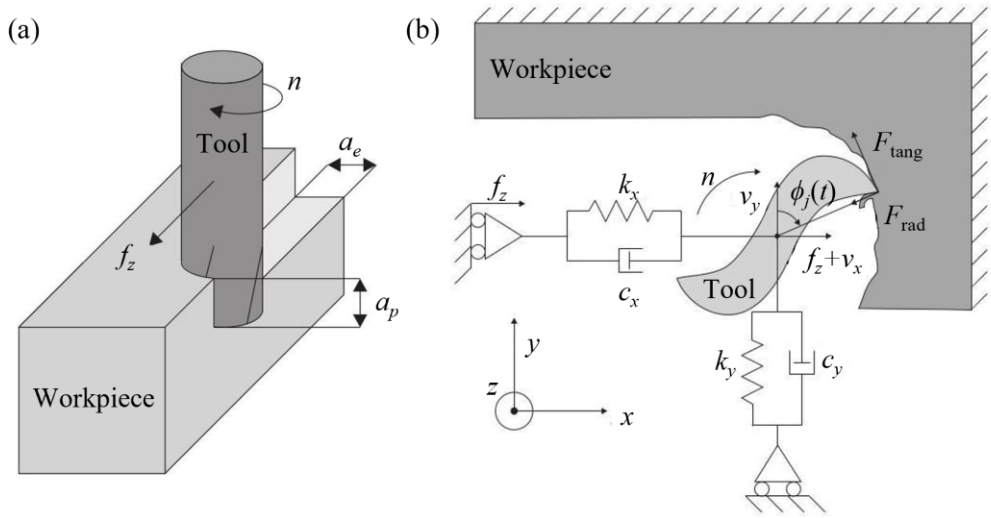

Fig. 4. Schematic of the milling process
(a) cutting parameters. (b) simplified two-dimensional milling model.

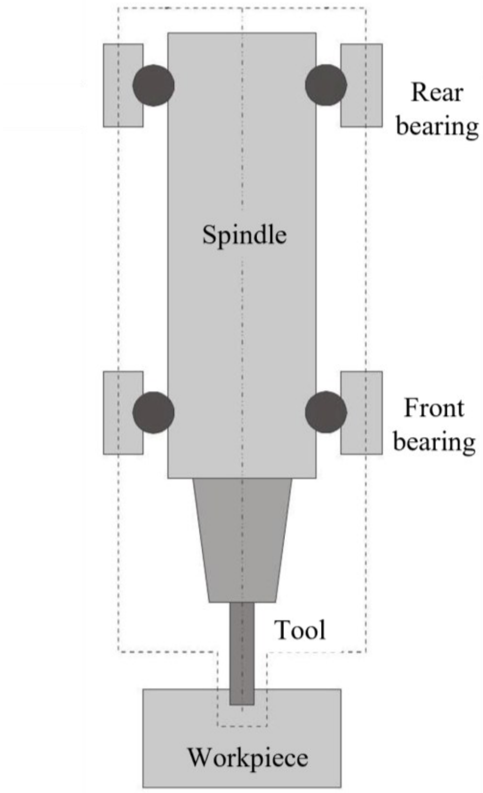

Fig. 5. Schematic of the spindle–holder–tool system

2.1.4 Time-delay milling model

Integrating chip thickness, cutting forces, and tool–spindle dynamics yields the governing delay differential equation (DDE) of milling. The spindle–tool dynamics are written as:

$$\dot{\boldsymbol{x}}(t) = \boldsymbol{A}\boldsymbol{x}(t) + \boldsymbol{B}\boldsymbol{F}(t) \tag{8}$$

$$\boldsymbol{v}(t) = \mathbf{C}\boldsymbol{x}(t) \tag{9}$$

The instantaneous chip thickness becomes

$$h_j(t) = h_{j,\text{ stat}}(t) + \begin{bmatrix} \sin\phi_j(t) & \cos\phi_j(t) \end{bmatrix} \left(\mathbf{C}\boldsymbol{x}(t) - \mathbf{C}\boldsymbol{x}\left(t - \tau_j(t)\right) \right) \tag{10}$$

with τ=60/(*zn*) the regenerative delay. Substituting this into the cutting-force model gives:

$$\begin{aligned} \boldsymbol{F}(t) = a_{\text{p}} \sum_{j=0}^{z-1} g_j\left(\phi_j(t)\right) \Big\{ h_{j,\text{ stat}}(t) + \\ \begin{bmatrix} \sin\phi_j(t) & \cos\phi_j(t) \end{bmatrix} \left(\mathbf{C}\boldsymbol{x}(t) - \mathbf{C}\boldsymbol{x}\left(t - \tau_j(t)\right) \right) \Big\}^{x_F} \quad \boldsymbol{S}(t) \begin{bmatrix} K_{\text{t}} \\ K_{\text{r}} \end{bmatrix} \end{aligned} \tag{11}$$

Finally, the closed system is:

$$\begin{aligned} \dot{\boldsymbol{x}}(t) = \boldsymbol{A}\boldsymbol{x}(t) + \boldsymbol{B} a_{\text{p}} \sum_{j=0}^{z-1} g_j\left(\phi_j(t)\right) \Big\{ h_{j,\text{ stat}}(t) + \\ \begin{bmatrix} \sin\phi_j(t) & \cos\phi_j(t) \end{bmatrix} \left(\mathbf{C}\boldsymbol{x}(t) - \mathbf{C}\boldsymbol{x}\left(t - \tau_j(t)\right) \right) \Big\}^{x_F} \quad \boldsymbol{S}(t) \begin{bmatrix} K_{\text{t}} \\ K_{\text{r}} \end{bmatrix} \end{aligned} \tag{12}$$

$$\boldsymbol{v}(t) = \mathbf{C}\boldsymbol{x}(t) \tag{13}$$

Equations (13)(14) define a time-varying delay differential equation (TV-DDE): current tool response depends not only on instantaneous displacement but also on its delayed history. This compact formulation embeds the regenerative effect and forms the basis for chatter prediction and suppression. As shown in Fig. 6, the chip thickness is represented by the nominal tooth path plus regenerative displacements, which drive cutting forces. These forces excite the spindle–holder–tool dynamics, whose delayed vibrations are fed back through time delay and coordinate transformation, thus closing the regenerative loop.

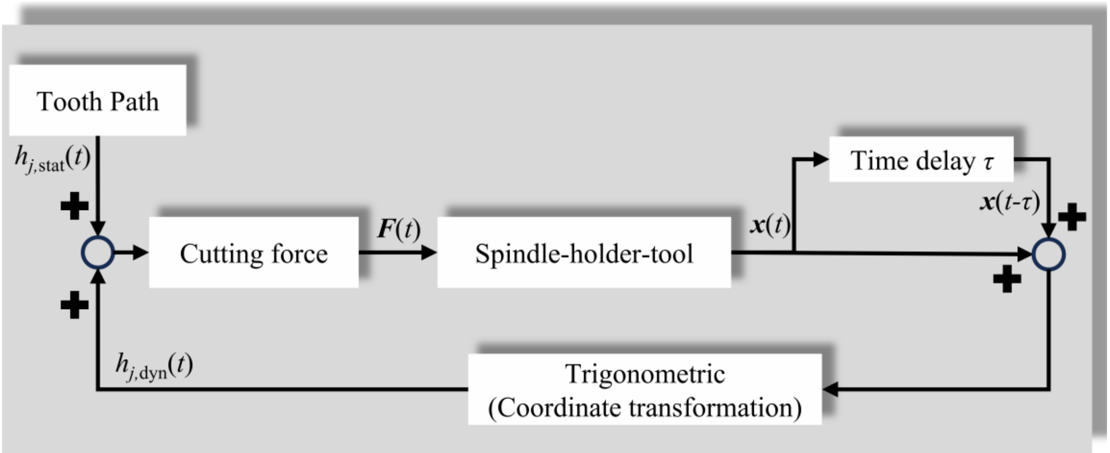

Fig. 6. System block diagram of milling process

2.1.5 Chatter frequency characteristics

The time-delay milling model not only describes the regenerative mechanism but also predicts clear spectral signatures. Because the excitation is periodic, the vibration response always contains deterministic frequency components that form the basis for chatter monitoring.

First, the spindle rotation frequency and its harmonics appear as

$$f_{\mathrm{SP}} = kf_{\mathrm{sp}} = k\frac{n}{60}, \quad k \in \mathbb{Z}^{+} \tag{14}$$

and the tooth-passing frequency and harmonics,

$$f_{\mathrm{TPE}} = kf_{\mathrm{tpe}} = k\frac{zn}{60}, \quad k \in \mathbb{Z}^{+} \tag{15}$$

reflect the periodic kinematics of the tool. These always appear in spectra, whether stable or unstable. The system's natural modes, most notably.

$$f_{\mathrm{d}} = \frac{\omega_0}{2\pi}\sqrt{1-\zeta^2} \tag{16}$$

add further peaks tied to spindle–tool dynamics.

When instability arises, additional components emerge. A secondary Hopf bifurcation generates sidebands,

$$f_{\mathrm{H}} = \pm f_{\mathrm{h}} + k\frac{n}{60}, \quad k \in \mathbb{Z} \tag{17}$$

producing a dominant chatter frequency f_{chat} usually near f_{d}. A period-doubling bifurcation yields fractional spindle harmonics,

$$f_{\mathrm{PD}} = \pm f_{\mathrm{pd}} + k\frac{n}{60}, \quad k \in \mathbb{Z} \tag{18}$$

so that 1/2 or 1/4 multiples of f_{sp} appear.

In practice, chatter progression can be tracked spectrally. In the stable stage, spectra are dominated by f_{sp}, f_{tpe}, and their harmonics. During initiation, sidebands or fractional harmonics appear, with f_{chat} typically near a structural mode. In the fully developed stage, energy at f_{chat} grows sharply, amplitudes diverge, and chatter marks form—often within 100 ms at high speeds.

Tool eccentricity complicates spectra by amplifying spindle harmonics and weakening tooth-passing components, but the emergence of fractional harmonics (e.g., 1/2 f_{sp} or 1/4 f_{sp}) remains a robust indicator of chatter onset. These frequency-domain signatures not only justify FFT–notch monitoring but also explain why spindle speed variation can be tuned to suppress regenerative feedback.

2.2 Real-time chatter monitoring

Effective chatter suppression requires fast and reliable onset detection. As established in Section 2.1, chatter introduces additional spectral components beyond the deterministic spindle and tooth-passing harmonics, motivating a frequency-domain strategy based on fast Fourier transform (FFT) with notch filtering.

Tool vibrations are measured by a triaxial accelerometer near the spindle bearing, sampled at 12.8 kHz. Short-time windows of about 100 ms balanced frequency resolution with computational speed. Each data segment $a(t)$ is detrended and normalized before analysis. The FFT is then applied to obtain the spectrum:

$$A(f) = \mathcal{F}\{a(t)\} \tag{19}$$

In stable cutting, $A(f)$ is dominated by spindle frequency f_{sp}=n/60, tooth-passing frequency f_{tpe}=zn/60, and their harmonics. To suppress these deterministic peaks, a notch filter is applied:

$$H(f) = \begin{cases} 0, & f \approx kf_{\mathrm{sp}}, kf_{\mathrm{tpe}} \\ 1, & \text{otherwise} \end{cases}, \quad k \in \mathbb{Z}^{+} \tag{20}$$

yielding the filtered spectrum:

$$A_{\mathrm{filtered}}(f) = A(f) \cdot H(f) \tag{21}$$

This isolates potential chatter frequencies. Onset is then declared when a filtered peak exceeds a threshold,

$$A_{\mathrm{filtered}}(f) \geq A_{\mathrm{th}} \tag{22}$$

where A_{th} is set empirically. Peaks near structural modes or fractional spindle harmonics are flagged as chatter-related, while deterministic components are excluded by design.

2.3 Adaptive spindle speed variation strategy

Chatter suppression is achieved by adaptively updating spindle speed based on the identified chatter frequency. The regenerative chip-thickness term is

$$h_{\mathrm{dyn}}(t) = v(t) - v(t-\tau) \tag{23}$$

with delay τ=60/(zn) determined by spindle speed n and tooth number z. Transforming Eq. (23) into the frequency domain yields

$$H_{\text{dyn}}(i\omega) = \left(1 - e^{-i\omega\tau}\right)V(i\omega) = Q(i\omega)V(i\omega) \tag{24}$$

where $Q(i\omega)=(1-e^{-i\omega\tau})$ acts as a frequency-domain filter. Its zeros satisfy

$$l\omega\tau = l\frac{\omega}{f_{\text{tpe}}}, \quad l = 0,1,2,\ldots \tag{25}$$

meaning that they occur exactly at the tooth-passing frequency $f_{\text{tpe}}=zn/60$and its harmonics. By adjusting spindle speed n, the delay τ shifts and moves these zero-locations. If the identified chatter frequency f_{chat} is brought close to one of them, the regenerative term in h_{dyn} is strongly attenuated, suppressing chatter growth.

Altintas and Budak's regenerative theory further formalizes this principle [49]. The phase relation between successive waves satisfies

$$\varepsilon + k = f_{\text{chat}}\frac{60}{zn} \tag{26}$$

where k is the lobe index and ε is the fractional phase difference. For maximum stability, ε should approach zero, meaning that successive tooth waves overlap in phase and the dynamic chip thickness vanishes. Setting ε=0 gives the admissible lobe index

$$k_{\text{new}} = \left\lfloor \frac{f_{\text{chat}} \cdot 60}{zn} \right\rfloor \tag{27}$$

with the corresponding stable spindle speed

$$n_{\text{new}} = \frac{60 f_{\text{chat}}}{k_{\text{new}} z} \tag{28}$$

In operation, once chatter is detected and f_{chat} identified, Eqs. (27) and (28) are applied to compute n_{new}, and the spindle is ramped to this value. Step size and acceleration are bounded to avoid overshoot across lobes, and incremental corrections can be repeated if system dynamics drift due to wear or thermal effects.

2.4 Experimental details

The experimental platform is built on an ABB IRB6700 200/2.6 industrial robot with a 200 kg payload, 2.6 m reach, and absolute positioning accuracy of 0.3 mm, as shown in Fig. 7. A high-speed spindle (DGZYX-12030/11A3-KFPWVS, 15 kW, maximum 30,000 rpm) is mounted on a custom support frame and stabilized by a water-circulation cooler maintaining 22 °C. Tooling consists of HSK-40E shrink-fit holders and 8 mm solid-carbide end mills designed for aluminum machining. The workpiece material is aluminum alloy EN AW-7075 with dimensions 150 × 150 × 15 mm, clamped on a cast-iron table (1.5 m × 1.0 m × 0.84 m, 1 t) to suppress external vibration.

Tool vibrations are measured by a PCB 356A24 tri-axial accelerometer (10 mV/g sensitivity, 1–9 kHz bandwidth, ±500 g range) mounted close to the spindle bearings. Signals are acquired using an NI 9234 dynamic data acquisition module (4 channels, 51.2 kS/s, ±5 V) installed in an NI cDAQ-9171 chassis and streamed to a host PC. A sampling rate of 12.8 kHz is used.

Spindle actuation is provided by a permanent-magnet synchronous drive commanded via a Siemens S7-1200 PLC, with TCP/IP communication to the host PC. Robot motion follows CAM-generated toolpaths executed in RobotStudio through RAPID code. Real-time monitoring and suppression are implemented in a MATLAB interface, which handles synchronous data acquisition, FFT–notch filtering, and adaptive spindle-speed updates at 100 ms intervals.

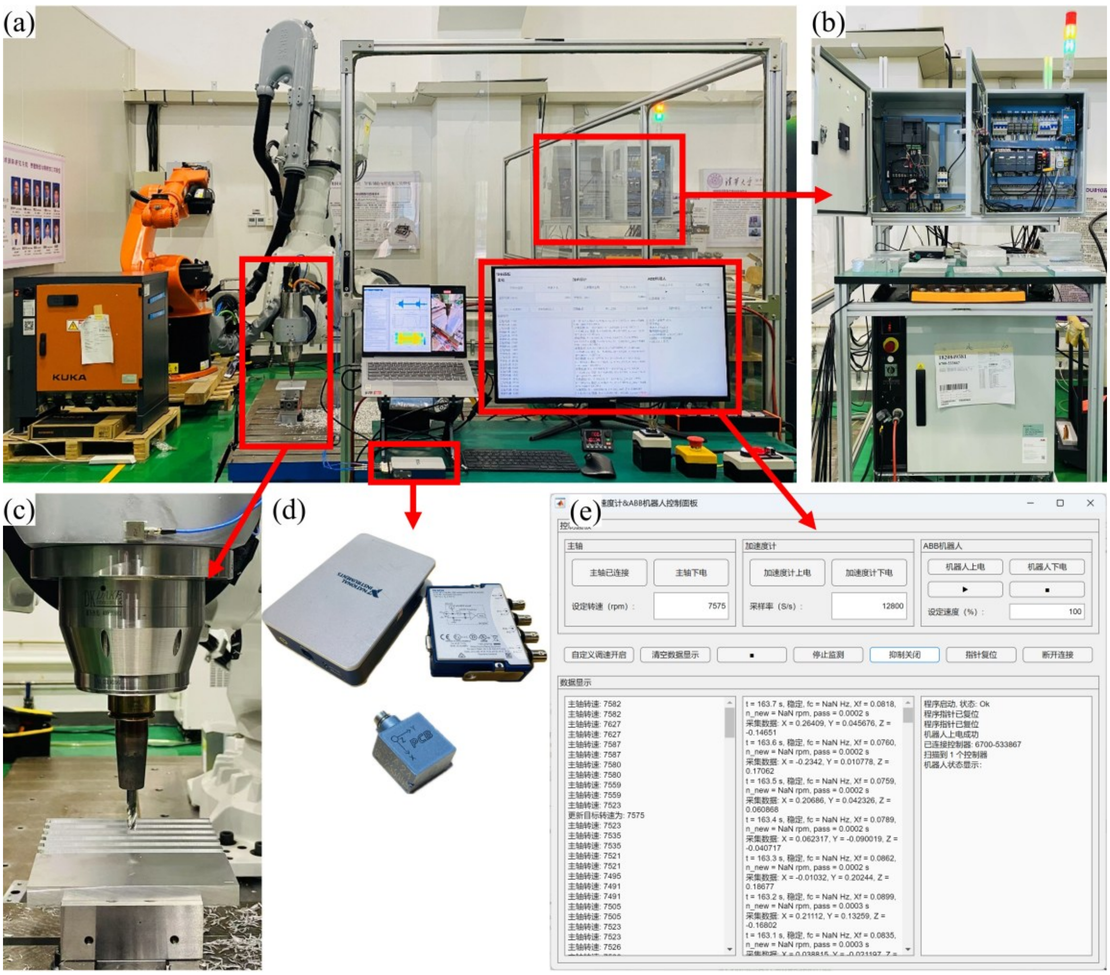

Fig. 7. Robotic milling system

(a) Full view. (b) Control system.

(c) Milling area. (d) NI DAQ & PCB Accelerometer. (e) MATLAB interface.

3 Results and discussion

3.1 Numerical validation of adaptive spindle speed variation

Numerical simulations are performed using the delay-differential milling model to validate the framework developed in section 2.1 and to assess chatter suppression by adaptive spindle speed variation (SSV) proposed in section 2.3. The spindle–tool system is represented as a two-degree-of-freedom mass–spring–damper oscillator, with cutting forces linearized for tractability. Dynamics are integrated tooth-by-tooth using MATLAB's solver (dde23). In the test scenario, spindle speed is set to 4520 rpm, then increased to 8200 rpm at 0.3 s and to 10,000 rpm at 0.6 s.

At the initial speed of 4520 rpm, vibration amplitudes diverge rapidly, exceeding ±1 mm within 0.3 s and reaching about ±2 mm by 0.7 s, as shown in Fig. 8. Increasing spindle speed to 8200 rpm stabilizes the response within ±1 mm, while a further increase to 10,000 rpm suppresses vibration to ±0.1 mm, corresponding to a reduction of more than 95 percent compared with constant speed. Fig. 9 demonstrates the corresponding state space representations: Poincaré points are widely scattered at 4520 rpm, become partially clustered at 8200 rpm, and converge to a near point attractor at 10,000 rpm. Time–frequency analysis in Fig. 10 further confirms these observations, where a dominant chatter peak around 670 Hz is visible at low speed, close to the system's natural frequency; after SSV updates, this peak disappears, leaving only tooth passing harmonics.

These results confirm that the milling model reproduces chatter onset and suppression accurately, and that adaptive SSV effectively disrupts the regenerative mechanism. The simulations therefore validate both the theoretical model and the control strategy, providing the basis for subsequent experimental evaluation.

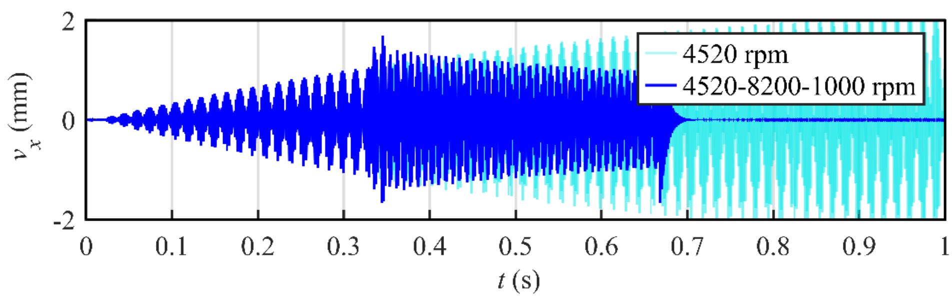

Fig. 8. Tool-tip displacement response in the time domain under variable spindle speed

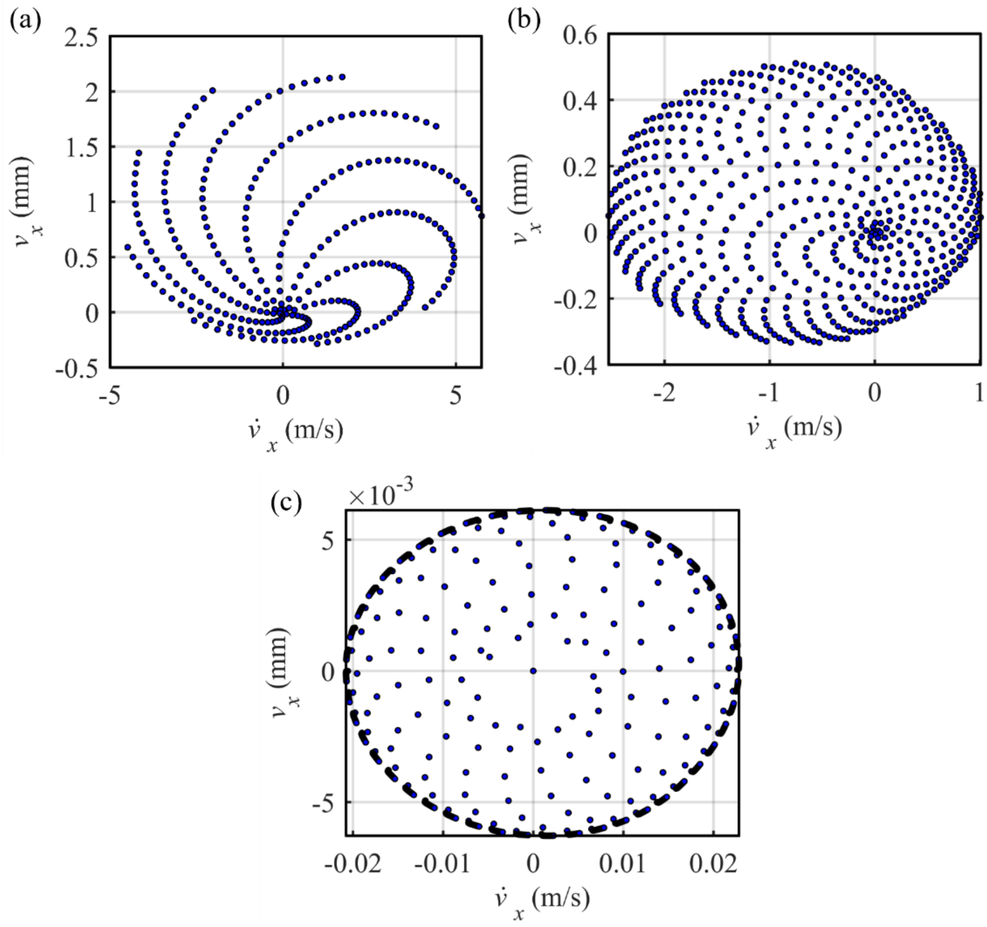

Fig. 9. State-space (Poincaré) maps based on tooth-period sampling
(a) 4520 rpm. (b) 8200 rpm. (c) 10,000 rpm

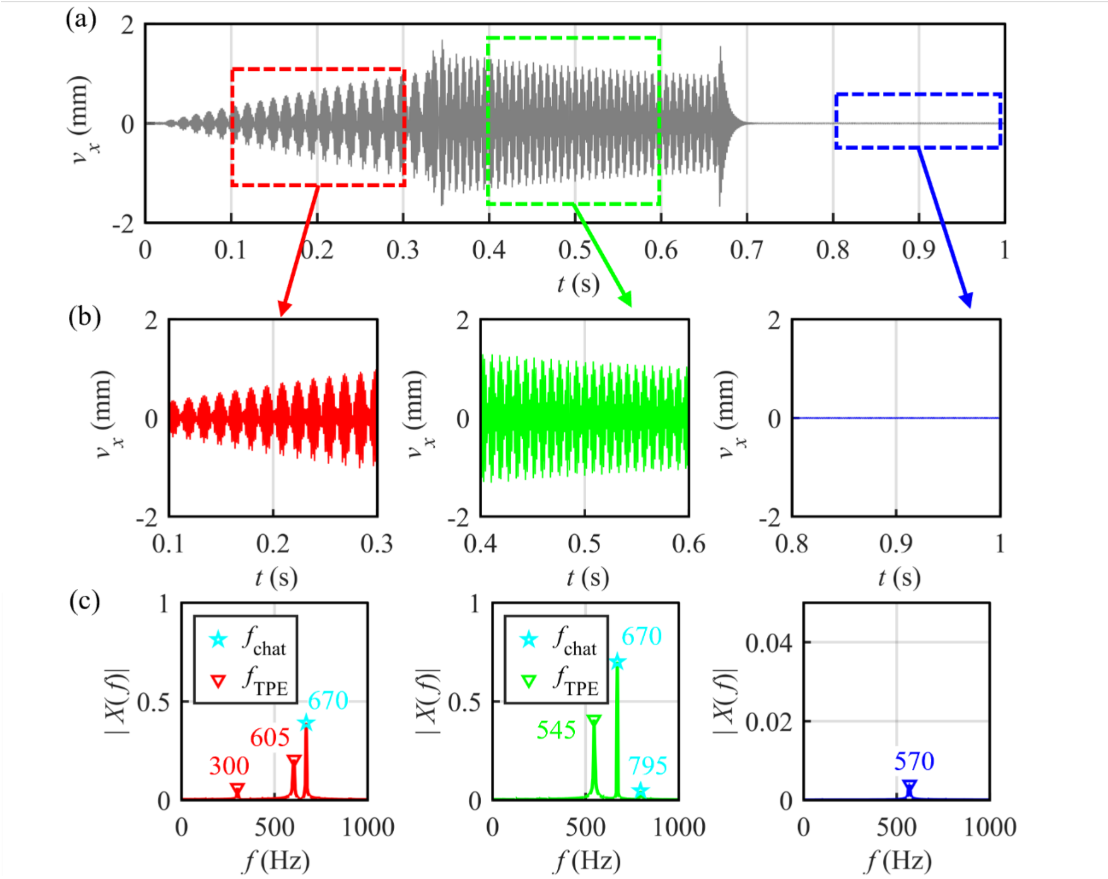

Fig. 10. Time–frequency analysis of tool-tip displacement at different spindle speeds (a) full time-domain response. (b) magnified view. (c) corresponding FFT spectra

3.2 Experimental validation on robotic milling

Slot-milling experiments are performed on aluminum blocks with a three-flute 8 mm cutter to validate chatter frequency identification and suppression. Fig. 11 compares representative spectra under stable and chatter conditions. In chatter cases (a,c,e), the dominant frequencies (188, 233, 278 Hz) clearly deviate from the spindle speed harmonics, whereas in stable cases (b,d,f), the dominant peaks align strictly with integer multiples of the spindle frequency (201, 84, 252 Hz). This one-to-one correspondence between frequency features and stability state confirms the utility of the chatter frequency characteristics in section 2.1.5 and demonstrates that spectral classification is reliable for robotic milling.

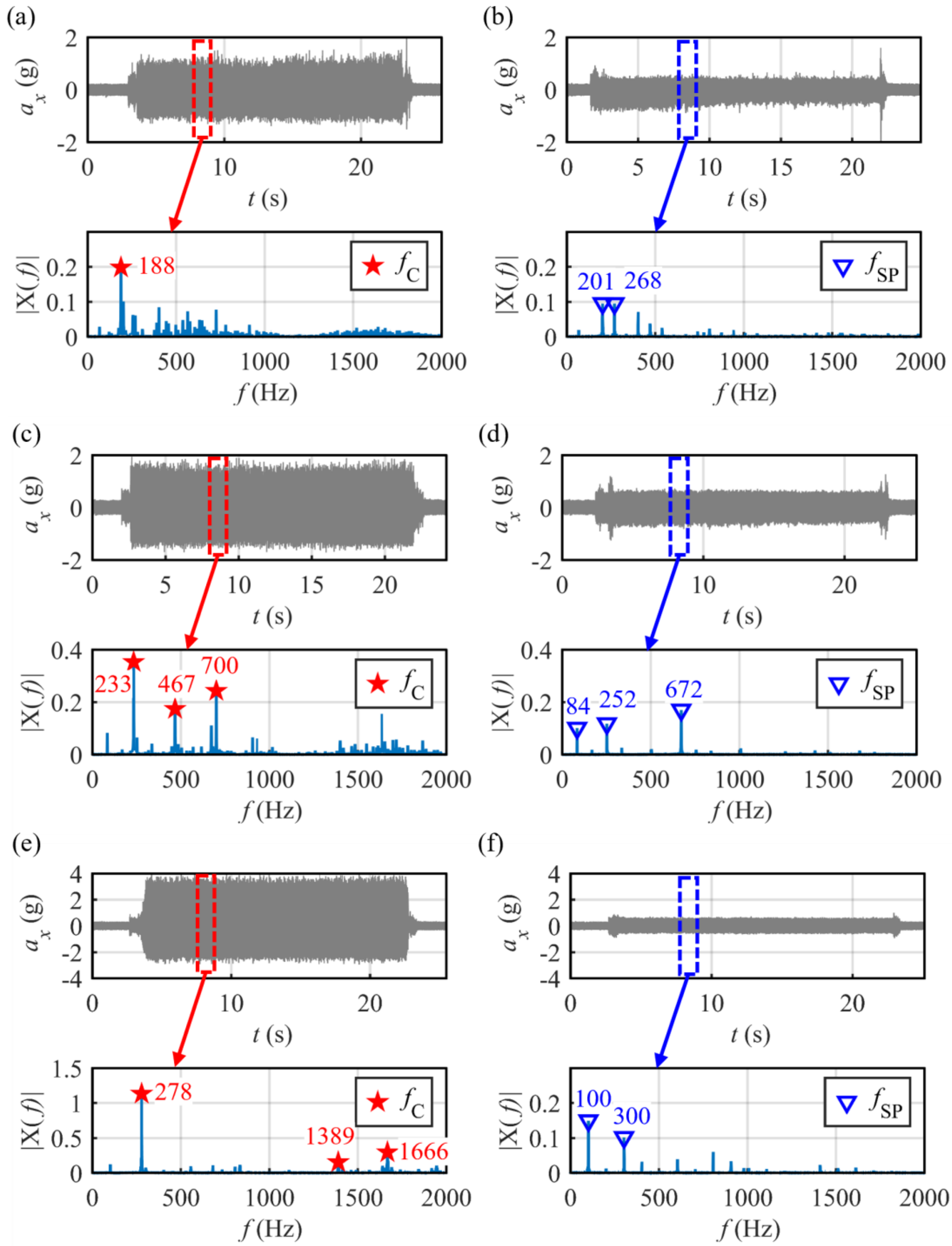

Fig. 11. Acceleration spectra under stable and chatter conditions

(a) n = 4000 rpm, a_p = 8 mm, f_{sp} = 66.7 Hz. (b) n = 4000 rpm, a_p = 7 mm, f_{sp} = 66.7 Hz.

(c) n = 5000 rpm, a_p = 8 mm, f_{sp} = 83.3 Hz. (d) n = 5000 rpm, a_p = 7 mm, f_{sp} = 83.3 Hz.

(e) n = 6000 rpm, a_p = 9 mm, f_{sp} = 100 Hz. (f) n = 6000 rpm, a_p = 8 mm, f_{sp} = 100 Hz.

To evaluate the practical effectiveness of adaptive spindle speed variation, slot milling tests are conducted under chatter-prone conditions (n=5000 rpm, a_p =8,9,10 mm). Based on Eqs. (27)(28), the spindle is accelerated to 7000 rpm, corresponding to the center of the neighboring stability lobe.

For a_p =10 mm, time- and frequency-domain responses (Fig. 12) show severe chatter at 5000 rpm, with a dominant off-harmonic peak at 234 Hz and its multiples. After the spindle accelerates to 7000 rpm at 15 s, vibration amplitudes drop sharply, and the spectrum is dominated by the spindle frequency (116.7 Hz) and its harmonics. Notably, the tooth-passing frequency at 7000 rpm coincides with the former f_{chat}, confirming the mechanism predicted in section 2.3.

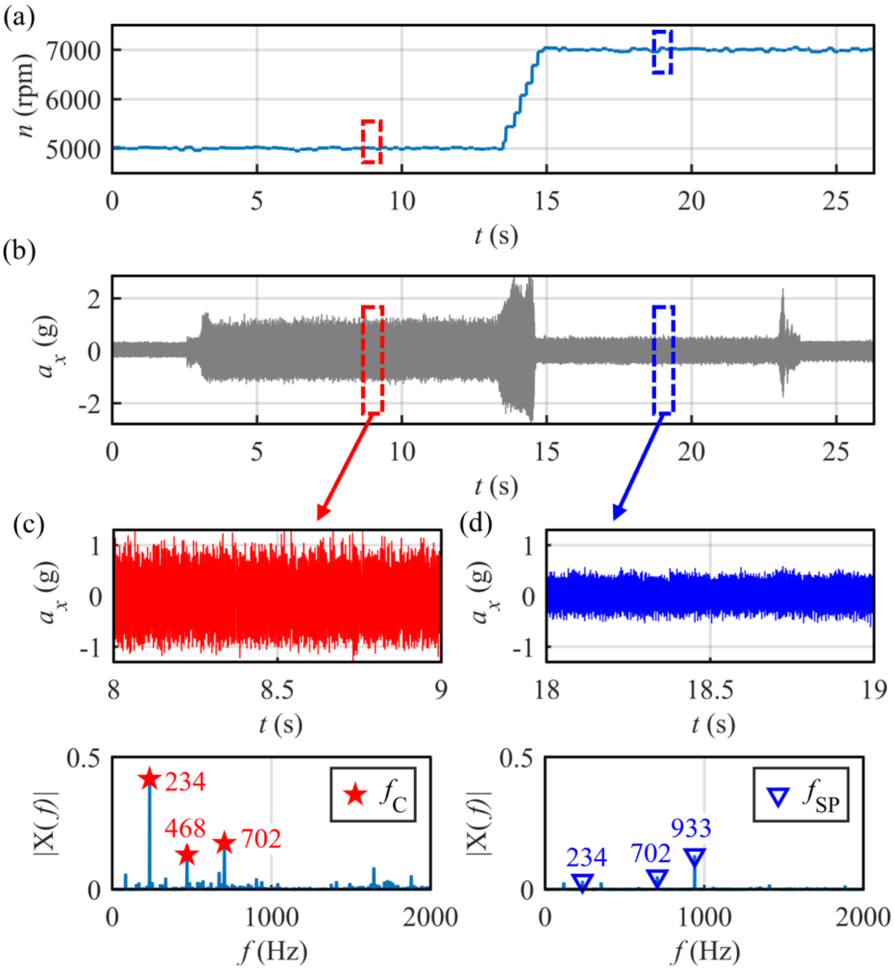

Fig. 12. Acceleration response from 5000 rpm to 7000 rpm
(a) spindle speed variation. (b) global time-domain signal.
(c) n = 5000 rpm, a_p = 10 mm, f_{sp} = 83.3 Hz. (d) n = 7000 rpm, a_p = 10 mm, f_{sp} = 116.7 Hz.

Surface roughness measurements further corroborate the suppression effect. As shown in Fig. 13, end-face roughness improves modestly from 3.0 μm to 2.5–2.8 μm due to limited stiffness in that direction, whereas side-wall roughness improves markedly from 1.6–2.0 μm to 0.5 μm, demonstrating that chatter-free cutting allows the robot system to approach ideal surface quality.

Closed-loop responsiveness is illustrated in Fig. 14, which provides a comprehensive view of real-time chatter detection and suppression through adaptive SSV. The raw acceleration $a_x(t)$ in the first row shows chatter growth and elimination, while the chatter state $C(t)$ in the second row switches from 0 (stable) to 1 (chatter) within 0.1–0.3 s after onset. The third row presents identified chatter frequencies $f_{\mathrm{chat}}(t)$; in Fig. 14(a), two dominant peaks, 240 Hz and 710 Hz, are captured, leading to calculated stable spindle speeds of 7500 rpm and 5250 rpm. The fourth row shows spindle response, where the blue curve n_{c} represents the actual speed and the gray curve n_{s} the target recomputed every 0.1 s. The fifth row displays the time–frequency map, where chatter-related peaks emerge during instability and vanish after spindle speed is updated.

Key timelines highlight responsiveness. In Fig. 14(a), milling begins at 2.6 s, chatter is detected at 2.9 s, SSV is activated at 4.8 s, and chatter is eliminated by 6.4 s, giving 1.6 s of combined detection–suppression time. In Fig. 14(b), milling begins at 15.8 s, chatter is detected at 16.8 s, SSV is activated at 18.3 s, and chatter disappears by 19.8 s, with a suppression duration of 1.5 s. Together these results confirm that chatter is detected promptly, corrective spindle speeds are computed almost instantaneously, ramping requires about 1 s, and chatter is fully suppressed within less than 2 s, demonstrating the responsiveness of the proposed FFT–SSV framework. Fig. 15 further demonstrates the overall effectiveness of chatter suppression through adaptive SSV.

Overall, these experiments demonstrate that adaptive SSV effectively suppresses chatter on a robotic milling platform, reduces vibration amplitudes, and improves surface finish, thereby validating both the theoretical mechanism and its practical feasibility.

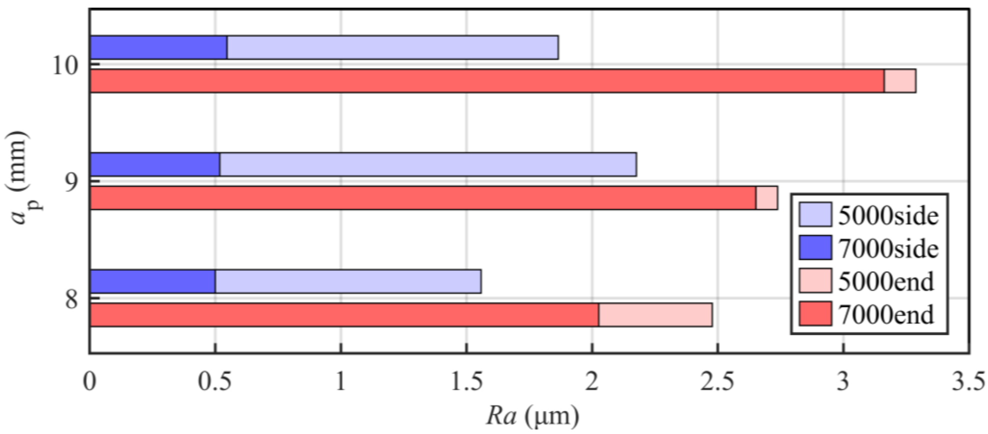

Fig. 13. Surface roughness *Ra* of end-face and side-wall before and after spindle speed increase from 5000 rpm to 7000 rpm

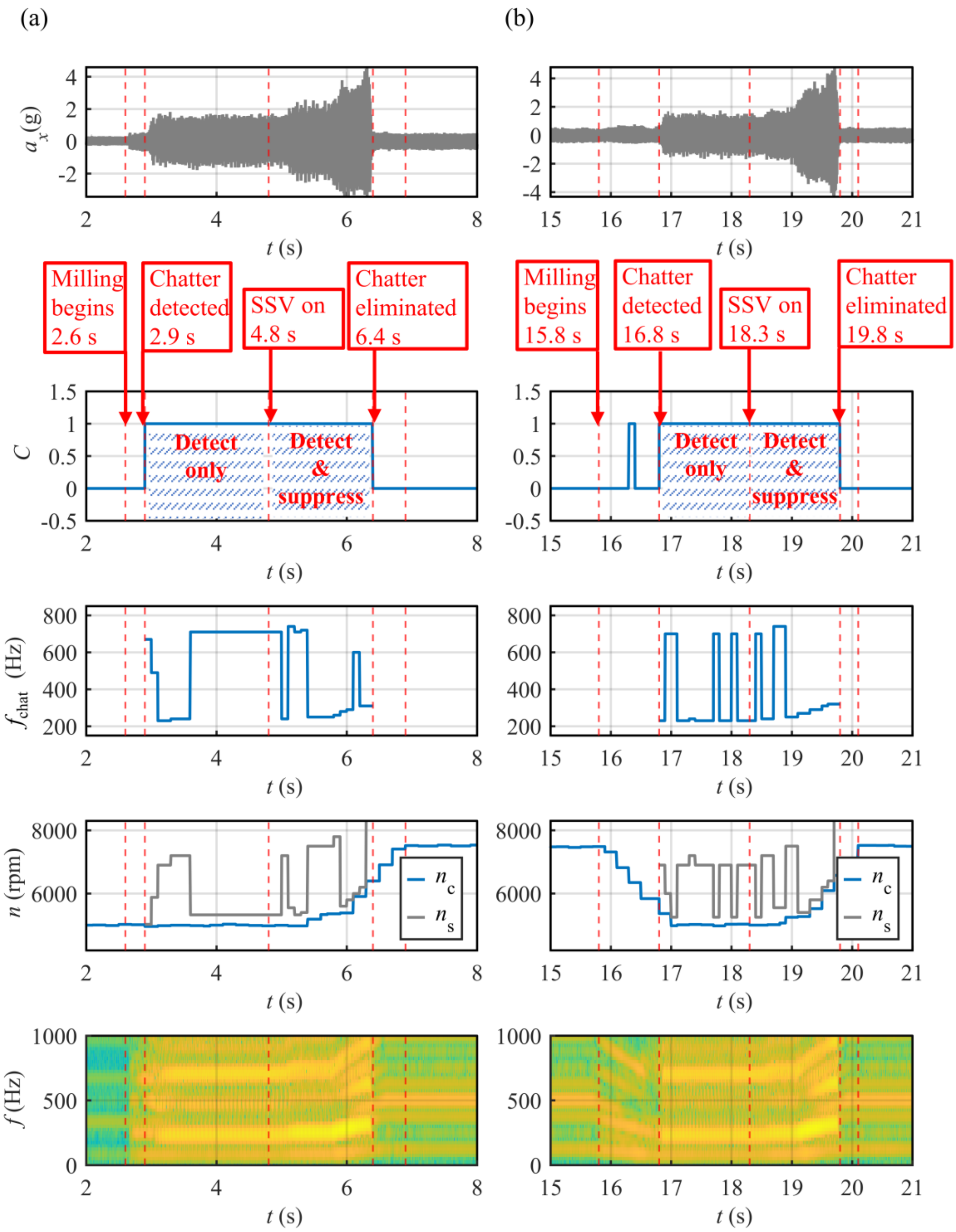

Fig. 14. Timeline of real-time chatter detection and suppression through adaptive SSV
Row 1: acceleration $a_x(t)$. Row 2: chatter state $C(t)$, 0 = stable, 1 = chatter. Row 3: identified chatter frequency $f_{chat}(t)$. Row 4: spindle speed with n_c (blue, actual) and n_s (gray, target).
Row 5: time–frequency map of $a_x(t)$.
(a) 2-8 s. (b) 15-21 s.

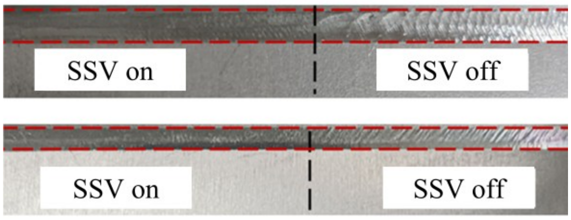

Fig. 15. Effectiveness of chatter suppression through spindle speed variation

4 Conclusions

1. This study establishes a real-time framework for chatter monitoring and suppression in robotic milling. A delay differential model captures the regenerative effect, explains the origin of chatter frequencies, and shows how spindle speed variation (SSV) disrupts feedback. Building on these insights, an FFT–notch scheme identifies chatter onset within milliseconds, and an adaptive SSV strategy updates spindle speed toward stability lobe centers.
2. Numerical simulations confirm that the model accurately reproduces chatter onset and suppression, and that adaptive SSV effectively attenuates regenerative vibrations. Experiments on an ABB IRB6700 robotic milling system further demonstrate reliable separation of chatter frequencies from spindle and tooth-passing harmonics, validating the spectral criteria. Suppression tests show that chatter is eliminated within about 1.6 s of detection, vibration amplitudes decrease by more than 90%, and side-wall surface roughness improves from roughly 2 μm to 0.5 μm.
3. These results imply that chatter suppression does not require structural modifications or auxiliary actuators. Leveraging only spindle speed updates guided by real-time spectral monitoring is sufficient to stabilize robotic milling. The proposed framework is lightweight, robust, and transferable to other machining platforms equipped with variable-speed spindles.

References

[1] H.E. Merritt, Theory of Self-Excited Machine-Tool Chatter: Contribution to Machine-Tool Chatter Research—1, J. Eng. Ind. 87 (1965) 447–454. https://doi.org/10.1115/1.3670861.

[2] M.K. Das, S.A. Tobias, The relation between the static and the dynamic cutting of metals, Int. J. Mach. Tool Des. Res. 7 (1967) 63–89. https://doi.org/10.1016/0020-7357(67)90026-1.

[3] J. Tlusty, M. Polacek, The stability of machine tools against self-excited vibrations in machining, Proc. ASME Int. Res. Prod. Eng. Conf. (1963) 465--474. DOI not available (1963 conference proceedings).
[4] N.K. Chandiramani, T. Pothala, Dynamics of 2-dof regenerative chatter during turning, J. Sound Vib. 290 (2006) 448–464. https://doi.org/10.1016/j.jsv.2005.04.012.
[5] Z.C. Wang, W.L. Cleghorn, Stability analysis of spinning stepped-shaft workpieces in a turning process, J. Sound Vib. 250 (2002) 356–367. https://doi.org/10.1006/jsvi.2001.3725.
[6] R. Mahdavinejad, Finite element analysis of machine and workpiece instability in turning, Int. J. Mach. Tools Manuf. 45 (2005) 753–760. https://doi.org/10.1016/j.ijmachtools.2004.11.017.
[7] S. Tangjitsitcharoen, In-process monitoring and detection of chip formation and chatter for CNC turning, J. Mater. Process. Technol. 209 (2009) 4682–4688. https://doi.org/10.1016/j.jmatprotec.2008.10.054.
[8] S. Tangjitsitcharoen, T. Moriwaki, Intelligent monitoring and identification of cutting states of chips and chatter on CNC turning machine, J. Manuf. Process. 10 (2008) 40–46. https://doi.org/10.1016/j.manpro.2008.01.001.
[9] F. Shi, H. Cao, X. Zhang, X. Chen, A Reinforced *k*-Nearest Neighbors Method With Application to Chatter Identification in High-Speed Milling, IEEE Trans. Ind. Electron. 67 (2020) 10844–10855. https://doi.org/10.1109/TIE.2019.2962465.
[10] J. Gradišek, A. Baus, E. Govekar, F. Klocke, I. Grabec, Automatic chatter detection in grinding, Int. J. Mach. Tools Manuf. 43 (2003) 1397–1403. https://doi.org/10.1016/S0890-6955(03)00184-6.
[11] W.K. Wang, M. Wan, W.H. Zhang, Y. Yang, Chatter detection methods in the machining processes: A review, J. Manuf. Process. 77 (2022) 240–259. https://doi.org/10.1016/j.jmapro.2022.03.018.
[12] P.S. Heyns, Tool condition monitoring using vibration measurements: a review, Insight - Non-Destr. Test. Cond. Monit. 49 (2007) 447–450. https://doi.org/10.1784/insi.2007.49.8.447.
[13] Y.S. Tarng, T.C. Li, M.C. Chen, On-line drilling chatter recognition and avoidance using an ART2—A neural network, Int. J. Mach. Tools Manuf. 34 (1994) 949–957. https://doi.org/10.1016/0890-6955(94)90027-2.
[14] O.V. Arriaza, Z. Tumurkhuyagc, D.-W. Kim, Chatter Identification using Multiple Sensors and Multi-Layer Neural Networks, Procedia Manuf. 17 (2018) 150–157. https://doi.org/10.1016/j.promfg.2018.10.030.

[15] Z. Yao, D. Mei, Z. Chen, On-line chatter detection and identification based on wavelet and support vector machine, J. Mater. Process. Technol. 210 (2010) 713–719. https://doi.org/10.1016/j.jmatprotec.2009.11.007.

[16] N. Lei, M. Soshi, Vision-based system for chatter identification and process optimization in high-speed milling, Int. J. Adv. Manuf. Technol. 89 (2017) 2757–2769. https://doi.org/10.1007/s00170-016-9770-2.

[17] O.O. Khalifa, A. Densibali, W. Faris, Image processing for chatter identification in machining processes, Int. J. Adv. Manuf. Technol. 31 (2006) 443–449. https://doi.org/10.1007/s00170-005-0233-4.

[18] W. Zhu, J. Zhuang, B. Guo, W. Teng, F. Wu, An optimized convolutional neural network for chatter detection in the milling of thin-walled parts, Int. J. Adv. Manuf. Technol. 106 (2020) 3881–3895. https://doi.org/10.1007/s00170-019-04899-1.

[19] M.H. Rahimi, H.N. Huynh, Y. Altintas, On-line chatter detection in milling with hybrid machine learning and physics-based model, CIRP J. Manuf. Sci. Technol. 35 (2021) 25–40. https://doi.org/10.1016/j.cirpj.2021.05.006.

[20] E. Marui, S. Ema, M. Hashimoto, Y. Wakasawa, Plate insertion as a means to improve the damping capacity of a cutting tool system, Int. J. Mach. Tools Manuf. 38 (1998) 1209–1220. https://doi.org/10.1016/S0890-6955(98)00001-7.

[21] N.H. Kim, D. Won, J.C. Ziegert, Numerical analysis and parameter study of a mechanical damper for use in long slender endmills, Int. J. Mach. Tools Manuf. 46 (2006) 500–507. https://doi.org/10.1016/j.ijmachtools.2005.07.004.

[22] R. Madoliat, S. Hayati, A. Ghasemi Ghalebahman, Investigation of chatter suppression in slender endmill via a frictional damper, Sci. Iran. 18 (2011) 1069–1077. https://doi.org/10.1016/j.scient.2011.08.008.

[23] R. Madoliat, S. Hayati, A.G. Ghalebahman, Modeling and Analysis of Frictional Damper Effect on Chatter Suppression in a Slender Endmill Tool, J. Adv. Mech. Des. Syst. Manuf. 5 (2011) 115–128. https://doi.org/10.1299/jamdsm.5.115.

[24] F.A.M. Galarza, M.V. De Albuquerque, A.Í.S. Antonialli, R. Pederiva, A.E. Diniz, Design and experimental evaluation of an impact damper to be used in a slender end mill tool in the machining of hardened steel, Int. J. Adv. Manuf. Technol. 106 (2020) 2553–2567. https://doi.org/10.1007/s00170-019-04786-9.

[25] V.R. Saciotto, A.E. Diniz, An experimental evaluation of particle impact dampers applied on the tool for milling of hardened steel complex surface, Int. J. Adv. Manuf. Technol. 119 (2022) 7579–7597. https://doi.org/10.1007/s00170-022-08782-4.

[26] N.A. Saadabad, H. Moradi, G. Vossoughi, Global Optimization and Design of Dynamic Absorbers for Chatter Suppression in Milling Process with Tool Wear and Process Damping, Procedia CIRP 21 (2014) 360–366. https://doi.org/10.1016/j.procir.2014.03.172.
[27] W. Ma, Y. Yang, X. Jin, Chatter suppression in micro-milling using shank-mounted Two-DOF tuned mass damper, Precis. Eng. 72 (2021) 144–157. https://doi.org/10.1016/j.precisioneng.2021.04.017.
[28] W. Ma, J. Yu, Y. Yang, Y. Wang, Optimization and Tuning of Passive Tuned Mass Damper Embedded in Milling Tool for Chatter Mitigation, J. Manuf. Mater. Process. 5 (2020) 2. https://doi.org/10.3390/jmmp5010002.
[29] X. Zhang, C. Wang, J. Liu, R. Yan, H. Cao, X. Chen, Robust active control based milling chatter suppression with perturbation model via piezoelectric stack actuators, Mech. Syst. Signal Process. 120 (2019) 808–835. https://doi.org/10.1016/j.ymssp.2018.10.043.
[30] J. Monnin, F. Kuster, K. Wegener, Optimal control for chatter mitigation in milling—Part 1: Modeling and control design, Control Eng. Pract. 24 (2014) 156–166. https://doi.org/10.1016/j.conengprac.2013.11.010.
[31] H.C. Möhring, P. Wiederkehr, C. Lerez, H. Schmitz, H. Goldau, C. Czichy, Sensor Integrated CFRP Structures for Intelligent Fixtures, Procedia Technol. 26 (2016) 120–128. https://doi.org/10.1016/j.protcy.2016.08.017.
[32] S. Wan, X. Li, W. Su, J. Yuan, J. Hong, X. Jin, Active damping of milling chatter vibration via a novel spindle system with an integrated electromagnetic actuator, Precis. Eng. 57 (2019) 203–210. https://doi.org/10.1016/j.precisioneng.2019.04.007.
[33] S. Wan, X. Li, W. Su, J. Yuan, J. Hong, Active chatter suppression for milling process with sliding mode control and electromagnetic actuator, Mech. Syst. Signal Process. 136 (2020) 106528. https://doi.org/10.1016/j.ymssp.2019.106528.
[34] J. Du, X. Liu, X. Long, Coupled LQG with robust control for milling chatter suppression, Int. J. Mech. Sci. 243 (2023) 108051. https://doi.org/10.1016/j.ijmecsci.2022.108051.
[35] H. Zhang, J. Ni, Internal Energy Based Analysis on Mechanism of Spindle Speed Variation for Regenerative Chatter Control, J. Vib. Control 16 (2010) 281–301. https://doi.org/10.1177/1077546309103562.
[36] M. Zatarain, I. Bediaga, J. Muñoa, R. Lizarralde, Stability of milling processes with continuous spindle speed variation: Analysis in the frequency and time domains,

and experimental correlation, CIRP Ann. 57 (2008) 379–384. https://doi.org/10.1016/j.cirp.2008.03.067.

[37] P. Albertelli, S. Musletti, M. Leonesio, G. Bianchi, M. Monno, Spindle speed variation in turning: technological effectiveness and applicability to real industrial cases, Int. J. Adv. Manuf. Technol. 62 (2012) 59–67. https://doi.org/10.1007/s00170-011-3790-8.

[38] C. Wang, X. Zhang, R. Yan, X. Chen, H. Cao, Multi harmonic spindle speed variation for milling chatter suppression and parameters optimization, Precis. Eng. 55 (2019) 268–274. https://doi.org/10.1016/j.precisioneng.2018.09.017.

[39] S. Nam, T. Hayasaka, H. Jung, E. Shamoto, Proposal of novel chatter stability indices of spindle speed variation based on its chatter growth characteristics, Precis. Eng. 62 (2020) 121–133. https://doi.org/10.1016/j.precisioneng.2019.11.018.

[40] Z. Li, Q. Song, Z. Liu, B. Wang, Y. Cai, Chatter suppression mechanism and parameters configuration of the spindle speed variation with piecewise characteristics, Int. J. Adv. Manuf. Technol. 122 (2022) 3041–3055. https://doi.org/10.1007/s00170-022-10071-z.

[41] S. Smith, J. Tlusty, Stabilizing Chatter by Automatic Spindle Speed Regulation, CIRP Ann. 41 (1992) 433–436. https://doi.org/10.1016/S0007-8506(07)61238-4.

[42] Y.S. Liao, Y.C. Young, A new on-line spindle speed regulation strategy for chatter control, Int. J. Mach. Tools Manuf. 36 (1996) 651–660. https://doi.org/10.1016/0890-6955(95)00076-3.

[43] Z. Han, H. Jin, D. Han, H. Fu, ESPRIT- and HMM-based real-time monitoring and suppression of machining chatter in smart CNC milling system, Int. J. Adv. Manuf. Technol. 89 (2017) 2731–2746. https://doi.org/10.1007/s00170-016-9863-y.

[44] S. Yamato, K. Nakanishi, N. Suzuki, Y. Kakinuma, Development of Automatic Chatter Suppression System in Parallel Milling by Real-Time Spindle Speed Control with Observer-Based Chatter Monitoring, Int. J. Precis. Eng. Manuf. 22 (2021) 227–240. https://doi.org/10.1007/s12541-021-00469-2.

[45] Z. Xiong, Online Chatter Detection and Suppression System for Intelligent Machine Tool, J. Mech. Eng. 54 (2018) 85. https://doi.org/10.3901/JME.2018.17.085.

[46] Y. Sun, Z. Xiong, An Optimal Weighted Wavelet Packet Entropy Method With Application to Real-Time Chatter Detection, IEEEASME Trans. Mechatron. 21 (2016) 2004–2014. https://doi.org/10.1109/TMECH.2016.2547481.

[47] N.J.M. Van Dijk, E.J.J. Doppenberg, R.P.H. Faassen, N. Van De Wouw, J.A.J. Oosterling, H. Nijmeijer, Automatic In-Process Chatter Avoidance in the High-

Speed Milling Process, J. Dyn. Syst. Meas. Control 132 (2010) 031006. https://doi.org/10.1115/1.4000821.

[48] H. Morita, T. Yamashita, Tracing and Visualizing Variation of Chatter for In-Process Identification of Preferred Spindle Speeds, Procedia CIRP 4 (2012) 11–16. https://doi.org/10.1016/j.procir.2012.10.003.

[49] Y. Altintas, Manufacturing automation: metal cutting mechanics, machine tool vibrations, and CNC design, 2nd ed, Cambridge University Press, Cambridge, 2012.